Nanoscale

Accepted Manuscript

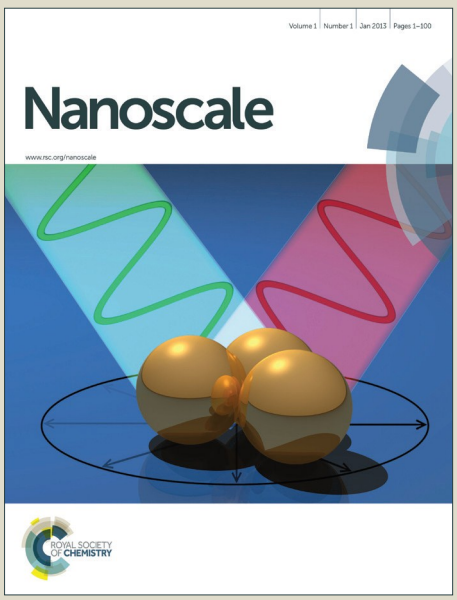

ROYAL SOCIETY OF CHEMISTRY

www.rsc.org/nanoscale

Journal Name

COMMUNICATION

Mid-infrared spectroscopy beyond the diffraction limit via direct measurement of photothermal effect

Received 00th January 20xx,
Accepted 00th January 20xx

DOI: 10.1039/x0xx00000x

www.rsc.org/

A. M. Katzenmeyer,[†] G. Holland,[†] J. Chae,[†‡] A. Band,[†] K. Kjoller[§] and A. Centrone[†*]

An atomic force microscope equipped with temperature sensitive probes was used to measure locally the photothermal effect induced by IR light absorption. This novel instrument opens a pathway to correlated topographical, chemical composition, and thermal mapping with nanoscale resolution. Proof of principle demonstration is provided on polymers and plasmonic samples.

Nanomaterials attract interest in applications ranging from electronics,[1] to biology,[2] and therapeutics[3] because they provide novel properties or improved performance with respect to their macroscopic counterparts.[3-6] However, harnessing their properties can be challenging because the ability to engineer and integrate nanomaterials in functional devices often depends on the availability of characterization methods for measuring material properties (electrical, chemical, thermal etc.) at the nanoscale. The atomic force microscope (AFM)[7] is a widely used characterization platform because, in addition to providing high resolution images of the sample topography, advanced AFM techniques can also provide local mechanical,[8] electrical,[9] thermal,[10-12] etc., properties of the sample. For example, scanning thermal microscopy (SThM)[10, 11, 13, 14] relies on probe tips with either a thermocouple or an electrically resistive element to obtain high resolution maps of the sample's thermal conductivity. Beginning more than 15 years ago, in an attempt to study chemical composition with a resolution smaller than the diffraction limit of IR light, pioneering work by Hammiche and coworkers combined a FTIR spectrometer with SThM.[15] This method, known as photothermal microspectroscopy (PTMS), typically relies on a broadband light source (globar) for illumination and on a Wollaston wire probe to locally measure the temperature increase in the sample due to light absorption. The photothermal signal is measured using a Wheatstone bridge (where the probe makes up one leg of the resistor bridge) and Fourier transformed to yield IR spectra with wavelength-independent resolution.[15] PTMS has been applied to characterize polymers,[15, 16] stem cells,[17] and cervical cancer cells.[18] However, to the best of our knowledge no chemical maps have been reported using this method. In addition to the direct light absorption in the tip,[16] the full potential of PTMS has been hindered by contrasting needs to improve its sensitivity (requiring bigger probes)[16] and its lateral resolution (requiring smaller probes).[19] Experiments using light sources with a higher brilliance and enabling a tighter focal spot than a globar, such as a synchrotron,[19] or an optical parametric oscillator[16] have provided better sensitivity, but have remained isolated attempts. The best PTMS results thus far claim ≈ 5 μm spatial resolution[19] and a sensitivity up to ≈ 65 μm^3 (≈ 100 fL).[20] Meanwhile thanks to recent advances, other scanning probe techniques such as photothermal induced resonance (PTIR)[21-24] and scattering scanning near-field optical microscopy,[25, 26] routinely measure IR spectra and maps providing chemical composition with nanoscale resolution. A recent review on this topic is available elsewhere.[27] However, none of these methods offers direct access to the sample's time-dependent thermal response; something that could be leveraged to extract the thermal conductivity of the sample. Although the PTMS signal may provide in principle such temporal information, the slow response time of the bulky Wollaston wire probes (≈ 100 μs)[15] has prevented this type of analysis.

In this work, we use nanofabricated resistive SThM probes[28] in combination with a modified commercially available PTIR set up[23, 29] to obtain IR spectra and maps with a lateral resolution as high as 70 nm, ≈ 70 times better than the estimated PTMS resolution. While the amplitude of the photothermal signal can provide the local chemical composition, its temporal evolution can be leveraged to derive the local sample thermal conductivity without a probe specific calibration, for samples with characteristic thermalization times longer than the response time of the probe (≈ 13 μs). These results are enabled by four concomitant factors: i) the use of SThM probes with a nanoscale tip radius (≈ 50 nm), ii) the use of a tunable pulsed source that induces local temperature changes on the order of tens of °C, iii) the use of total internal reflection illumination that minimizes the direct absorption of light by the probe, and iv) sample preparation enabling rapid thermalization (thin sample). We name this new technique scanning thermal infrared microscopy (STIRM). One of the advantages of this novel approach is the acquisition of correlated topographic, SThM, and PTIR (chemical

[†]Center for Nanoscale Science and Technology, National Institute Standards and Technology, Gaithersburg, Maryland 20899, USA
[‡]Maryland Nanocenter, University of Maryland, College Park, MD 20742, USA
[§]Anasys Instruments Inc.,325 Chapala Street, Santa Barbara, CA 93101, USA
[*]E-mail: andrea.centrone@nist.gov

composition) data in addition to the STIRM signal. We suggest that by measuring temperature (instead of expansion), STIRM will complement the chemical imaging capability of PTIR for very thin (< 50 nm) samples or for materials with a small thermal expansion coefficient that are, for PTIR, typically more challenging to measure.[29]

As shown in figure 1a, in our setup monochromatic light pulses illuminate the sample (on top of a transparent prism) via total internal reflection to minimize direct interaction with the probe. Such an illumination scheme requires that the sample be prepared on an IR-transparent prism. In PTIR, the AFM tip transduces locally the sample's thermal expansion, due to light absorption, into cantilever oscillations which are detected in the far-field by reflecting a diode laser into the AFM detector (figure 1a). The PTIR signal is generated by the following transduction chain: sample absorption, sample heating, sample expansion, AFM cantilever deflection, and optical readout by the AFM detector. The temporal spacing between the laser pulses (1 ms) allows the sample and cantilever to return to equilibrium well before the arrival of the following pulse. Because of the short laser pulse (10 ns here) and the rapid thermalization of the (thin) sample, the cantilever excitation is much faster than the characteristic response time of the AFM topography feedback loop. Consequently, for thin samples, the temporal evolution of the PTIR signal (Figure 1b) is mostly determined by the temporal response of the cantilever rather than by the thermal properties of the sample. For example, the characteristic thermalization time for the polymer and gold samples analyzed here, ranges from ≈ 100 µs to ≈ 40 ps, much shorter than the cantilever ringdown (figure 1b).

For the current study we replace the typical contact mode probe used in PTIR with a commercially available nanofabricated scanning thermal microscopy (SThM) probe[28] (figure 1a). The thermal sensing element consists of a thin film resistor (40 nm Pd on 5 nm NiCr) approximately 1 µm wide, which is patterned along the periphery of the silicon nitride support. The total resistance of the probe is typically 320 Ω; 200 Ω of which are contributed by two series resistors on the cantilever. The inset of fig. 1 shows a simplified schematic of the circuitry used. A battery powered voltage regulator biases a Wheatstone bridge where $R_1 = R_2 = 600\ \Omega$. R_{ADJ} is tuned to match the probe resistance, R_{PROBE}, after contacting the sample. The output voltage, V_0, of a differential amplifier (20 dB gain) can be additionally amplified, if desired, before being routed to an oscilloscope or the instrument's controller. The differential amplifier was operated at a reduced 100 kHz (of 100 MHz) bandwidth to increase the signal to noise ratio, unless otherwise noted. To obtain a sufficiently large signal, the probe is typically operated with a current between 2.25 mA to 2.5 mA. In this "active" mode of operation, the heat generated in the probe is dissipated by the environment and sample. With respect to steady state, the transient photothermal heating of the sample reduces (or suppresses) the heat transfer from the tip to sample, effectively increasing the tip temperature and consequently increasing the probe resistance. The STIRM signal (figure 1c) is derived from the following transduction chain: sample absorption, sample heating, probe resistance increase, electrical readout. As in PTIR, the steady state and transient signals may be recorded concurrently; the difference being that the SThM steady state produces a qualitative map of the sample's thermal conductivity rather than topography.

As proof of principle we measure samples with very different thermo-mechanical properties, three polymer samples and a sample consisting of thin gold plasmonic resonators. The latter was chosen because it is challenging to measure with the PTIR technique.[30] Among the three polymer samples, *sample-1* is a poly methyl-methacrylate (PMMA) film annealed at 180 °C with thickness ranging from 1600 nm ± 10 nm to 3000 nm ± 10 nm, as determined by AFM. Uncertainties through the manuscript represent a single standard deviation. *Sample-2* and *sample-3* are microtomed films consisting of PMMA particles embedded in an epoxy matrix with thicknesses of ≈ 300 nm and of ≈ 1000 nm, respectively. Figure 1c shows the output voltage, V_o, obtained by illuminating *sample-1* at 1720 cm^{-1}, corresponding to the carbonyl stretching absorption. The transient signal is rather simple to interpret qualitatively and opens a new pathway for mapping both the chemical composition and the thermal properties of the sample. The signal decay in figure 1c is well fit by an equation of the form $e^{-t/t_{relax}}$ with a single characteristic relaxation time, $t_{relax} = C\rho z^2/\kappa = 25.6\,\mu s \pm 1.3\,\mu s$ where t is time, C is the specific heat capacity, ρ is the density of the material, z is the thickness of the material, and κ is the thermal conductivity. Because the intrinsic relaxation time for the probe is sufficiently fast (≈ 13 µs, see Fig. S1 of supporting information), by measuring the sample height (z = 1620 nm ± 10 nm in 1c) we can extract the sample's thermal diffusivity, $D_{th} = \kappa/C\rho$. Because C and ρ are known for PMMA,[31] we derive $\kappa = 0.16 \pm 0.01$ $W{\cdot}m^{-1}{\cdot}K^{-1}$, in good agreement with the bulk value. Values of t_{relax} and κ extracted from measurements on *sample-1* at location with different thickness are given in table ST1 of the supplemental material.) The uncertainty of κ is mainly determined by the uncertainty in the sample thickness and fitting. The STIRM thermal conductivity uncertainty (≈ 6%) compare well with the uncertainty typically obtainable with the time-domain thermo-reflectance technique (≈ 10 %) for measuring thermal conductivity at the macroscale. Consequently, a quantitative determination of the sample's thermal conductivity can be made in cases where the thermal relaxation time of the sample exceeds that of the probe, overcoming some of the limitations of steady state SThM characterization. These include drift in the probe temperature due to environment or electrical offsets and the inherent noise limitations of DC measurements. Additionally, assessing κ with SThM typically requires extensive and tip specific calibration and it is possible only for samples with $0.2 < \kappa < 10$ $W{\cdot}m^{-1}{\cdot}K^{-1}$.[32]

The other polymer samples studied have relaxation times which are too fast for similar analysis (≈ 1 µs for *sample-2* and ≈ 8 µs for *sample-3*); however, improving the response time by an order of magnitude may make such studies feasible. A thermal sensor with a smaller time constant could be obtained by reducing the sensor mass by means of e-beam lithography or post fabrication focused ion beam milling. Nonetheless the maximum amplitude of the signal, as for PTIR, can be used to construct absorption spectra and chemical maps.

Figure 1d shows spectra of *sample-2* obtained with the probe placed on a PMMA particle (green) and the surrounding epoxy (black). The height image is shown in Figure 1e and the

corresponding chemical images of PMMA (f, 1720 cm^{-1}, carbonyl stretching absorption) and epoxy (g, 1604 cm^{-1}, C=C stretching absorption). To the best of our knowledge these maps constitute the first demonstration of sub diffraction chemical imaging using resistive probes as near-field detectors. To better quantify the STIRM resolution we used the thicker *sample-3* to improve signal to noise ratio. Figure 2 shows the normalized line traces for height (black) and STIRM signal (green) obtained for wavelengths absorbed by epoxy (a) and by PMMA (b) as identified by the dashed lines of the color-coded maps (insets). The height data show that the PMMA particle does not have very abrupt edges which hinders the assessment of the resolution. As a very conservative estimate we note that the signal decay from 80 % to 20 % of the maximum for the epoxy data occurs within 176 nm ± 32 nm, limited by non-abrupt epoxy-PMMA interface. However, the comparison of full-width half maxima[33] yields $|FWHM_{HEIGHT} - FWHM_{STIRM}|$ = 60 nm ± 36 nm suggesting a nanoscale resolution on the order of the pixel size, 70 nm here. While images in figure 1 and 2 exhibit resolution higher than the diffraction limit, the correlation with the boundaries in the height image is markedly better for the epoxy than for the PMMA chemical maps. In first approximation, this observation may be surprising because PMMA and epoxy have similar thermal conductivities.[34] However, the difference in resolution can be rationalized by considering the thermal contact of the two phases with the environment. The PMMA surface is rough, with undulations exceeding 100 nm, which preclude an efficient thermal contact with the substrate, likely broadening the thermal profile, when compared to good thermal contact. Conversely, the smooth epoxy is expected to make efficient thermal contact to the prism, and yield a better lateral resolution. In contrast, for thin samples heat diffusion typically does not negatively affect the lateral resolution of PTIR maps so drastically[23] (see figure S2).

We qualitatively understand this as follows. In STIRM, the signal amplitude is a direct measure of the local maximum temperature, which may not present large discontinuities at interphases. In PTIR the signal intensity is instead mediated by the transduction of heat into mechanical expansion and into the cantilever ring-down oscillation (figure 1b). Because of the different signal transduction in PTIR, we can identify three contributions favoring higher resolution for PTIR in this particular case (i.e. absorption in PMMA and heat diffusion to the epoxy phase): i) the PTIR signal is proportional to z^3, $(z_{epoxy}/z_{PMMA})^3 \approx 0.73$,[22] ii) the PTIR signal is proportional to the sample expansion coefficient (α), $\alpha_{epoxy}/\alpha_{PMMA} \approx 0.28$[35, 36] and iii) because the heat diffusion is much slower than the laser pulses (10 ns) the resulting thermal expansion is not fast enough to excite the fastest oscillation modes in the cantilever as efficiently and should result in a reduced cantilever ringdown amplitude. Although, the latter effect is difficult to quantify a priori, this analysis suggests that at the interface, for a given temperature, the PTIR signal on the epoxy side would be at most ≈ 10 % the value on the PMMA side, resulting in a sharp signal discontinuity (contrast) at the interphase.

We also investigated gold asymmetric split ring resonators (ASRRs) prepared by e-beam lithography and lift-off. Because of unfavorable thermomechanical properties, gold samples are typically challenging to measure with the PTIR technique.[30] The ASSRs studied here are 57 nm ± 2 nm thick, as determined by AFM, and despite exhibiting far-field IR reflectance spectra similar to thicker resonators characterized previously,[30] they were too thin to yield a suitable signal for extensive PTIR characterization without damaging the sample. Nevertheless, the STIRM probe can measure these thin resonators and shows similar spectra (figure 3a) to those obtained by PTIR for thicker samples.[30]

The STIRM maps similarly show a crossover from predominant excitation of the shorter right arc for higher frequencies (figure 3b, 1500 cm^{-1}) to the longer left arc (figure 3d at 1300 cm^{-1}) beyond the crossover frequency of 1400 cm^{-1} (3c) at which both arcs are similarly excited. However, the PTIR maps observed previously showed a rather homogenous signal throughout the excited arc(s), resulting from the thermal expansion due to Ohmic dissipation (see also Fig S3). In contrast, figure 3 show a clearly different signal distribution – which we attribute to the electric-field intensity driving the dissipative currents responsible for the PTIR signal. We arrive at this conclusion considering the rapid thermalization time of the gold sample (40 ps) and the very large local fields, which induce self-absorption in the tip, which is otherwise negligible in absence of the resonators. Because the SThM probe can also be used for PTIR, the two complementary data sets may prove useful, whenever measurable concomitantly, to engineer plasmonic devices providing information on the field distribution and Ohmic loss.

Conclusions

This work introduces a new method for measuring mid-IR absorption spectra and maps with a lateral resolution surpassing the diffraction limit, by directly measuring the heat resulting from light absorption in the sample. The STIRM setup described here provides a considerable step forward with respect to previous PTMS works and allows to record concurrently topographical, SThM, and PTIR maps without compromising performance. By measuring temperature (in addition to expansion), STIRM can complement the PTIR chemical imaging capabilities for very thin samples or for samples with small thermal expansion coefficients. Preliminary data suggest that it is possible to quantitatively extract the local thermal diffusivity or even the local thermal conductivity (if ρ, C are known) from the STIRM signal provided the temporal evolution of the signal is sample-limited. In general, for unknown samples the local thermal diffusivity measured with STIRM could be translated into thermal conductivity values by leveraging the local PTIR spectrum for material identification and by leveraging the macroscale ρ, C literature data for the identified material. Improving the probe response time could enable such measurements for a larger variety of samples (i.e. thinner, or with larger thermal conductivity). Lastly, we show the efficacy of STIRM in determining the near-field response of plasmonic structures.

References

1 A. J. Huber, J. Wittborn and R. Hillenbrand, *Nanotechnology*, 2010, **21**, 235702
2 D. C. Fernandez, R. Bhargava, S. M. Hewitt and I. W. Levin, *Nat. Biotechnol.*, 2005, **23**, 469-474.
3 L. J. Zhang and T. J. Webster, *Nano Today*, 2009, **4**, 66-80.
4 C. Lee, X. D. Wei, J. W. Kysar and J. Hone, *Science*, 2008, **321**, 385-388.
5 D. G. Cahill, W. K. Ford, K. E. Goodson, G. D. Mahan, A. Majumdar, H. J. Maris, R. Merlin and Phillpot, Sr., *J. Appl. Phys.*, 2003, **93**, 793-818.
6 Y. Yuan, J. Chae, Y. Shao, Q. Wang, Z. Xiao, A. Centrone and J. Huang, *Advanced Energy Materials*, 2015, DOI: 10.1002/aenm.201500615.
7 G. Binnig, C. F. Quate and C. Gerber, *Phys. Rev. Lett.*, 1986, **56**, 930-933.
8 O. Sahin, S. Magonov, C. Su, C. F. Quate and O. Solgaard, *Nat. Nanotechnol.*, 2007, **2**, 507-514.
9 R. A. Oliver, *Rep. Prog. Phys.*, 2008, **71**, 076501.
10 A. Majumdar, *Annu. Rev. Mater. Sci.*, 1999, **29**, 505-585.
11 A. I. Buzin, P. Kamasa, M. Pyda and B. Wunderlich, *Thermochim. Acta*, 2002, **381**, 9-18.
12 B. A. Nelson and W. P. King, *Rev. Sci. Instrum.*, 2007, **78**.
13 M. E. McConney, D. D. Kulkarni, H. Jiang, T. J. Bunning and V. V. Tsukruk, *Nano Lett.*, 2012, **12**, 1218-1223.
14 K. Kim, J. Chung, G. Hwang, O. Kwon and J. S. Lee, *ACS Nano*, 2011, **5**, 8700-8709.
15 A. Hammiche, H. M. Pollock, M. Reading, M. Claybourn, P. H. Turner and K. Jewkes, *Appl. Spectrosc.*, 1999, **53**, 810-815.
16 L. Bozec, A. Hammiche, H. M. Pollock, M. Conroy, J. M. Chalmers, N. J. Everall and L. Turin, *J. Appl. Phys.*, 2001, **90**, 5159-5165.
17 O. Grude, T. Nakamura, A. Hammiche, A. J. Bentley, F. L. Martin, H. M. Pollock, S. Kinoshita and N. J. Fullwood, *Vib. Spectrosc.*, 2009, **49**, 22-27.
18 M. J. Walsh, M. J. German, M. Singh, H. M. Pollock, A. Hammiche, M. Kyrgiou, H. F. Stringfellow, E. Paraskevaidis, P. L. Martin-Hirsch and F. L. Martin, *Cancer Lett*, 2007, **246**, 1-11.
19 L. Bozec, A. Hammiche, M. J. Tobin, J. M. Chalmers, N. J. Everall and H. M. Pollock, *Meas. Sci. Technol.*, 2002, **13**, 1217-1222.
20 A. Hammiche, L. Bozec, H. M. Pollock, M. German and M. Reading, *Journal of Microscopy*, 2004, **213**, 129-134.
21 A. Dazzi, R. Prazeres, F. Glotin and J. M. Ortega, *Ultramicroscopy*, 2007, **107**, 1194-1200.
22 B. Lahiri, G. Holland and A. Centrone, *Small*, 2013, **9**, 439-445.
23 A. M. Katzenmeyer, G. Holland, K. Kjoller and A. Centrone, *Anal. Chem.*, 2015, **87**, 3154-3159.
24 J. R. Felts, K. Kjoller, M. Lo, C. B. Prater and W. P. King, *ACS Nano*, 2012, **6**, 8015-8021.
25 F. Huth, A. Govyadinov, S. Amarie, W. Nuansing, F. Keilmann and R. Hillenbrand, *Nano Lett.*, 2012, **12**, 3973-3978.
26 M. B. Raschke, L. Molina, T. Elsaesser, D. H. Kim, W. Knoll and K. Hinrichs, *ChemPhysChem*, 2005, **6**, 2197-2203.
27 A. Centrone, *Annual Review of Analytical Chemistry*, 2015, DOI: 10.1146/annurev-anchem-071114-040435.
28 G. Mills, H. Zhou, A. Midha, L. Donaldson and J. M. R. Weaver, *Appl. Phys. Lett.*, 1998, **72**, 2900-2902.
29 A. M. Katzenmeyer, V. Aksyuk and A. Centrone, *Anal. Chem.*, 2013, **85**, 1972-1979.
30 A. M. Katzenmeyer, J. Chae, R. Kasica, G. Holland, B. Lahiri and A. Centrone, *Adv. Opt. Mater.*, 2014, **2**, 718-722.
31 U. Gaur, S. F. Lau, B. B. Wunderlich and B. Wunderlich, *J. Phys. Chem. Ref. Data*, 1982, **11**, 1065-1089.
32 H. Fischer, *Thermochim. Acta*, 2005, **425**, 69-74.
33 A. M. Katzenmeyer, G. Holland, K. Kjoller and A. Centrone, *Anal. Chem.*, 2015, **87**, 3154-3159.
34 Y. Yang, in *Physical Properties of Polymers Handbook*, ed. J. E. Mark, AIP Press, 1996.
35 A. Yasmin and I. M. Daniel, *Polymer*, 2004, **45**, 8211-8219.
36 C. Y. Zhi, Y. Bando, W. L. Wang, C. C. Tang, H. Kuwahara and D. Golberg, *Journal of Nanomaterials*, 2008, **2008**, 5.

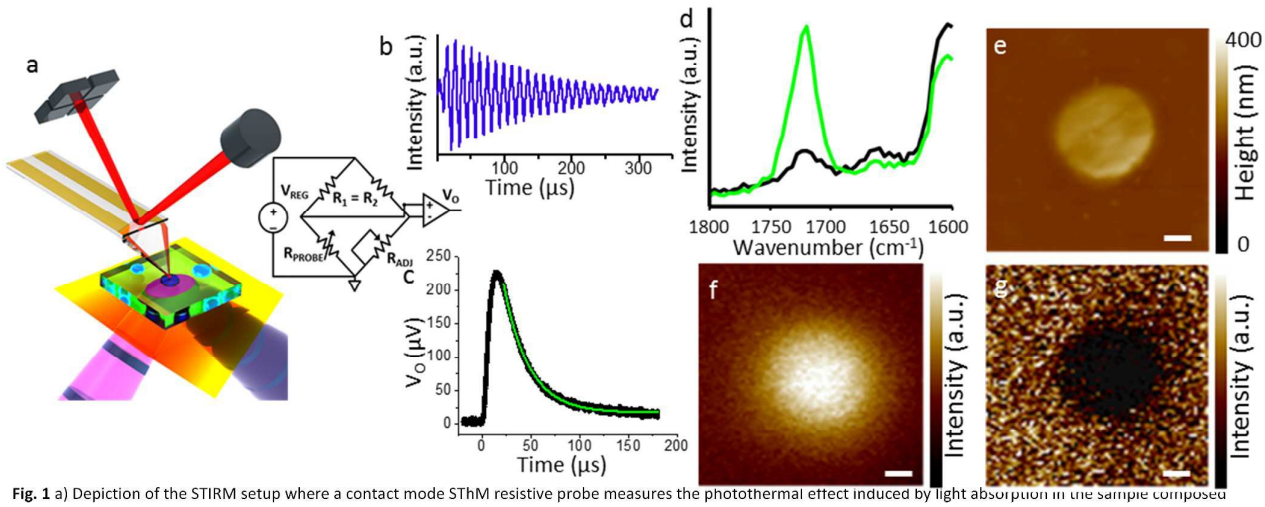

Fig. 1 a) Depiction of the STIRM setup where a contact mode SThM resistive probe measures the photothermal effect induced by light absorption in the sample composed of PMMA particles (blue) dispersed in an epoxy matrix (green). Simplified schematic of the STIRM circuitry (inset); the output voltage (V_0) signal is proportional to change in probe resistance (R_{PROBE}), which is in turn proportional to the sample temperature and to the absorbed energy. b) Typical PTIR ringdown signal showing induced cantilever oscialltions. c) Transient output voltage (V_0) averaged over 6.53 x 10^4 laser pulses resulting from the optical excitation of *sample-1* recorded with 1 MHz bandwidth. The green line is an exponential fit to the signal decay. d) STIRM Spectra of a PMMA particle of *Sample-2* (green) and adjacent epoxy (black). Spectra were recorded by averaging the signal of 256 consecutive pulses per wavelength and tuning the laser in intervals of 4 cm^{-1}. e) AFM height image and corresponding STIRM maps of f) PMMA (1720 cm^{-1}) and g) epoxy (1604 cm^{-1}). Pixel size is 100 nm x 100 nm and each pixel was obtained by averaging the signal of 128 laser pulses. Scale bars are 1 μm.

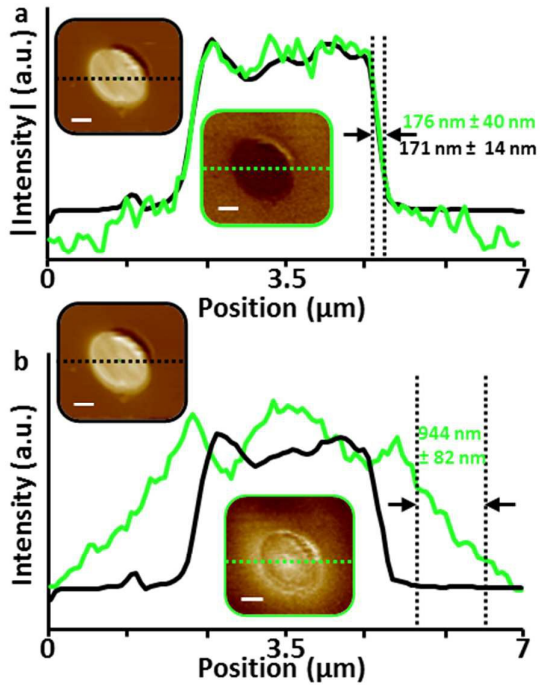

Fig. 2 Sample-3. a,b) Normalized height (black) and STIRM (green) line profiles of a) epoxy (1604 cm^{-1}), the STIRM trace was inverted for ease of comparison, and b) PMMA (1720 cm^{-1}). The profiles represent the average of 5 lines taken at the locations indicated by the dashed lines in the respective images (insets). The STIRM images were recorded by averaging the response over 32 laser pulses. Image pixels are 70 nm x 70 nm. Scale bars are 1 μm.